Electronic Supplementary Information

Highly stretchable and sensitive strain sensor based on graphene-elastomer composites with a novel double-interconnected network

Yong Lin, Shuqi Liu, Song Chen, Yong Wei, Xuchu Dong, Lan Liu*

College of Materials Science and Engineering, Key Lab of Guangdong Province for High Property and Functional Macromolecular Materials, South China University of Technology, Guangzhou 510640, P. R. China

* Corresponding author. E-mail: *psliulan@scut.edu.cn* Tel: +86 20-87114857.

Experimental

Materials

NR latex (NRL) with a total solid content of 60 wt% was supplied by Maoming Shuguang Rubber Farm. SBR latex (SBRL, Intex 132, solid content of 60 wt %, styrene content is 25 wt%), was manufactured by Lanzhou Petrochemical Co. Ltd. Graphite powder was purchased from Shanghai Colloidal Co. Ltd. Poly(diallyldimethylammonium chloride) (PDDA) was purchased from Sinopharm Chemical Reagent Co., Ltd. Calcium chloride ($CaCl_2$) and hydrazine hydrate was provided by Guangzhou Chemical Reagent Factory. Octyl phenol 10 (OP-10) was supplied by Sinopharm Chemical Reagent Co. Ltd. Rubber additives such as zinc oxide (ZnO), stearic acid (SA), N-cyclo-hexylbenzothiazole-2-sulphenamide (CZ), 2,2'-dibenzothiazole disulfide (DM), 2-Mercaptobenzimidazole (MB) and sulfur (S) were obtained from Guangzhou Longsun technology Co., Ltd. All the rubber ingredients were industrial grade and were used as received.

Preparation of PDDA functionalized graphene (*f*-GE)

Graphite oxide (GO) was firstly synthesized according to our previous work[1]. *f*-GE was then prepared by reducing GO with hydrazine hydrate in the presence of PDDA. Specifically, 0.5 g GO was well dispersed in 200 ml water to produce the homogeneous graphene oxide (GO) suspensions, followed by the addition of 0.8 g PDDA to obtain a homogeneous dispersion by a sonication process. Afterwards, 900 μL hydrazine hydrates was added into the obtained homogeneous dispersion and the mixed solution was then subjected to a chemical reduction

reaction at 95 °C in an oil bath for 2 h to obtain a homogeneous black suspension.

Preparation of SBR/NR composites

The SBR/NR composites were prepared by a latex compounding technology. Typically, the above-obtained *f*-GE suspension was diluted to the appropriate amounts of *f*-GE aqueous suspension, accompanied with sonication for 1 h. Then, NRL, SBRL and vulcanized aqueous suspension (the crosslinking agent sulphur and other rubber additives) was uniformly mixed with the *f*-GE suspension under intense stirring. Subsequently, the mixtures were poured into an acetic solution tank, causing the coagulation. Then, the obtained solids were filtrated and washed repeatedly with deionized water, and then vacuum dried in an oven at 55 °C for 24 h. After that, the dried solid compounds were compress molded at 150 °C for cure time (T_{90}) under a pressure of 10 MPa. The obtained composites with a double-interconnected network were coded as SBR/NR-GE-x. For comparison, un-modified graphene was employed to prepare SBR/NR composites without a double-interconnected network following the similar procedure, which was coded as SBR/NR/GE-x. Herein, x represents the *f*-GE or GE content as parts per hundred parts of rubber, which was controlled to be 0, 0.25, 0.5, 0.75, 1.0, 2.0 and 4.0 phr (parts per hundred parts of rubber) in the composites. The formulation of the SBR composite is listed in Table S1.

Characterization

Transmission electron microscopy (TEM) was performed on a JEOL2100 microscope. Scanning electron microscopy (FESEM) was analyzed by a Nova NANOSEM 430. Fourier transform infrared spectroscopy (FT-IR) was recorded on a Bruker Vertex Fourier Transform Infrared Spectrometer. Thermogravimetric analysis (TGA) was collected on a Netzsch TG209F1 apparatus with a heating rate of 20 °C/min under nitrogen atmosphere. Zeta potential measurements were performed using a Zetasizer Nano-ZS. Tensile test experiments were measured by a U-CAN UT-2060 instrument at room temperature with a cross head speed of 500 mm/min. The electrical conductivity of all samples was measured by a two-point measurement using a digital source-meter according to our previous work[2]. The resistance change in the stretching-releasing process was measured according to our previous work[3-4]. The stretching process and stretching-releasing process of the samples were conducted at room temperature using a digital force gauge (CK-50HB, Fuzhou Aipu Instruments Co., Ltd) with a constant strain rate, and the strain rate can be adjusted from 0 to 40 min^{-1}. In the experiment, the strain rate was set as 4 min^{-1}. Accordingly, the

corresponding resistance changes of the samples during the stretching or releasing process were recorded using a TEGAM 1740 micro ohmmeter (data acquisition rate was 20 s^{-1}). Notice that two copper sheets were attached tightly on the samples with clamps for tightly contacting the test samples. In the test, the micro-ohmmeter was used to record the initial resistance (R_0) and real-time resistance (R) under strain. Then the resistance changes shown in the manuscript ((R-R_0)/R_0=$\Delta R/R_0$) was obtained by data conversion. The detailed device architecture can be shown in the Fig. S1.

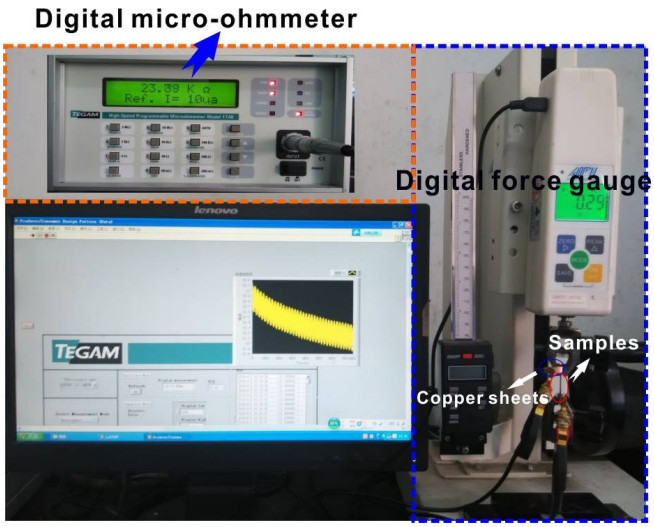

Fig. S1 Digital photograph of device architecture including digital micro-ohmmeter and digital force gauge.

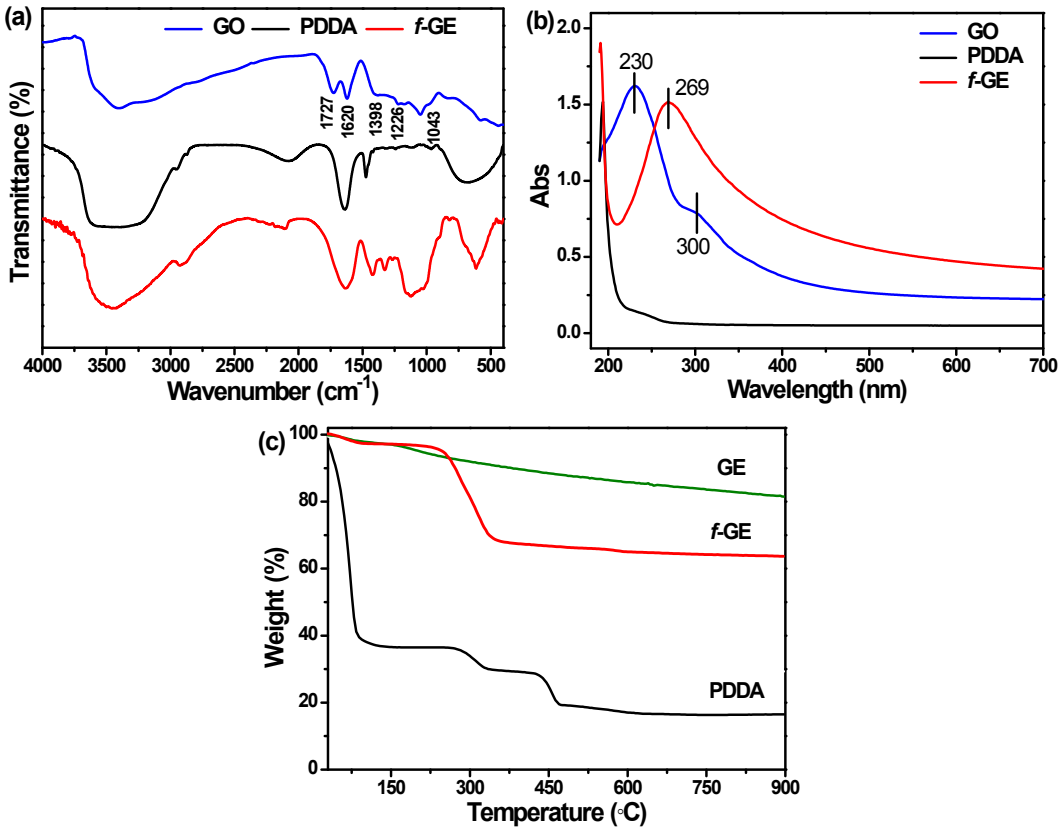

Fig. S2 FT-IR spectra (a) and UV-Vis spectra (b) of GO, PDDA and *f*-GE; (c) TGA curves of GE, PDDA and *f*-GE.

Fig. S2(a) shows the FT-IR spectroscopy results of GO, PDDA and *f*-GE. The peaks located at 1043, 1226, 1398, 1620, 1727 cm^{-1} in the GO spectrum are assigned to C-O stretching vibrations, C-OH stretching band, C-O-H deformation band, C=C stretching vibrations, and C=O stretching of COOH groups, respectively, suggesting the existence of hydroxyl, carboxyl, and epoxide groups on the surface of GO. With regard to the PDDA and *f*-GE, The two spectrums of the samples show the $-CH_2-$ deformation vibration around 1470 cm^{-1}, and the bending vibration of adsorbed water molecules located at 1630 cm^{-1}. Notably, those peaks ascribed to the oxygen-containing functional groups are not observed, suggesting the efficient reduction of GO. Furthermore, we used UV-vis spectrum to characterize the GO, PDDA and *f*-GE, as shown in Fig. S2(b). Pure PDDA shows no characteristic peak in the spectrum. As for GO, two characteristic peaks at 230 and 300 nm are observed, respectively. The peak at 230 nm of GO shifts to 269 nm for *f*-GE, indicating that GO is effectively reduced.

Fig. S2(c) shows the TGA curves of GE, *f*-GE. The slight weight loss occurs at 30~900 °C for GO, corresponding to the loss of the residual oxygen-containing groups onto the GE sheets. For

pure PDDA, PDDA starts to lose weight (60.5%) even below 90 °C, and exhibits decomposition behavior (9.5% weight loss) as the temperature increases from 250 to 360 °C because of the labile pendant groups on the main-chains. Another observed drop (13% weight loss) occurs at 380~610 °C, which is due to the pyrolysis of the carbon skeleton of PDDA. With respect to *f*-GE, the mass loss of *f*-GE largely decreases, suggesting the effective functionalization of GE by PDDA. The residual weight implies that the grafted PDDA content onto the GE sheets is about 18.0 wt%.

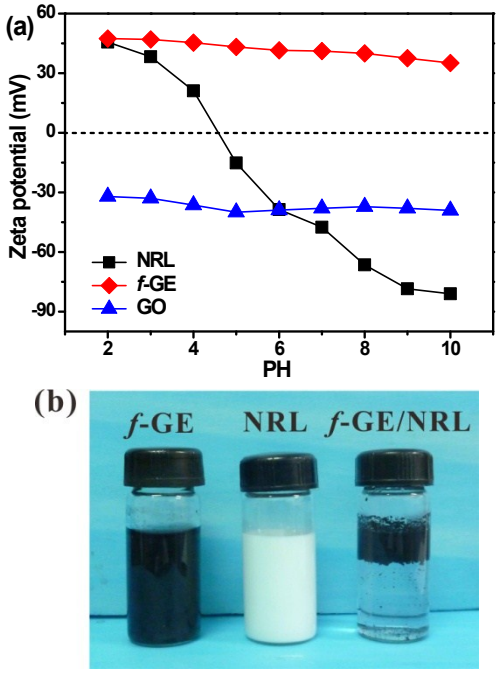

Fig. S3 (a) Zeta potentials of NRL, GO and *f*-GE as a function of pH. (b) Digital photographs of NRL, *f*-GE and *f*-GE/NRL containing of 0.42 vol% *f*-GE.

Zeta potential measurement was employed to verify the assembly process between *f*-GE and NRL, the results were shown in Fig. S3. It is evident that GO sheets possess a negatively charged surface (zeta potential = -30 mV ~ -40 mV) at the PH range from 2 to 10, which is due to the ionization of carboxylic acid and hydroxyl groups on the GO sheets[5]. After functionalized by PDDA, *f*-GE present a positively charged surface (zeta potential = +35 ~ +48 mV). Regarding to NRL, owing to the existence of the adsorbed amphiprotic proteins[6,7], its surface charge switches from positive (zeta potential = +45.6 mV) to negative (zeta potential = -81.0 mV). Herein, the pH conditions is selected at PH=6, where the assembly process can be successfully occurred between NRL (negative charge with zeta potential of -38.6 mV) and *f*-GE (positive charge with zeta potential of +41.5 mV), and we observed an ideal assembly that almost all the NRL particles are encapsulated with GE sheets, leaving a transparent aqueous sublayer (Fig. S3(b)).

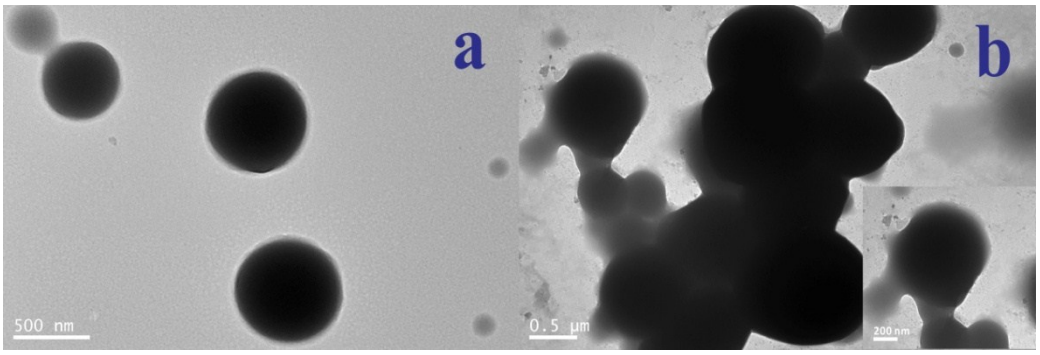

Fig. S4 Typical TEM images of NRL (a) and *f*-GE/NRL (b).

TEM observations provide visual evidence for the assembly. As shown in Fig. S4(a), neat NRL particles with diameters of 200-1000 nm exhibit smooth un-textured surfaces. As for NRL/*f*-GE (Fig. S4b), *f*-GE compactly encapsulated NRL particles were observed due to a strong electrostatic attraction interaction.

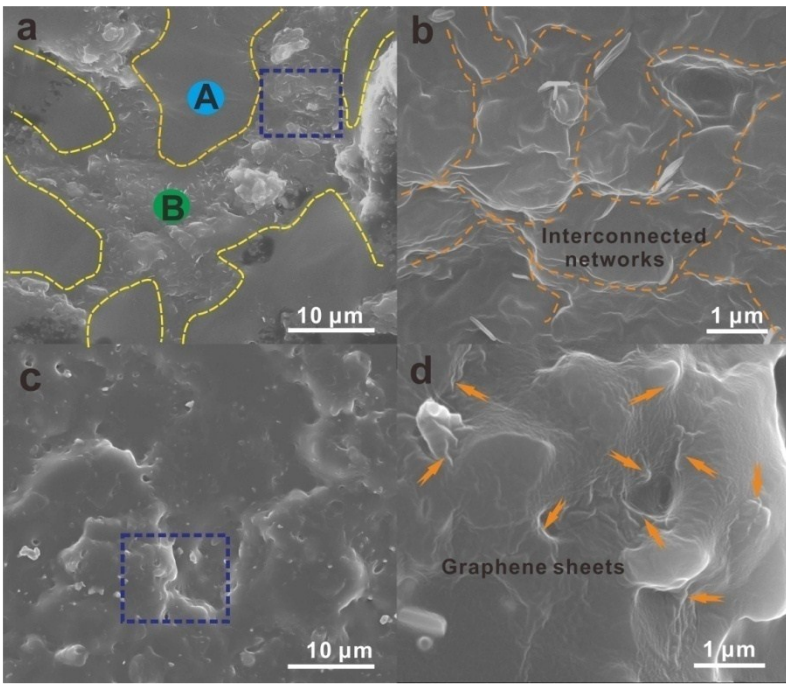

Fig. S5 Typical SEM images of SBR/NR-GE-0.42 (a,b) and SBR/NR/GE-0.42 (c,d). Region A corresponds to the SBR phase and region B represents the NR phase containing *f*-GE.

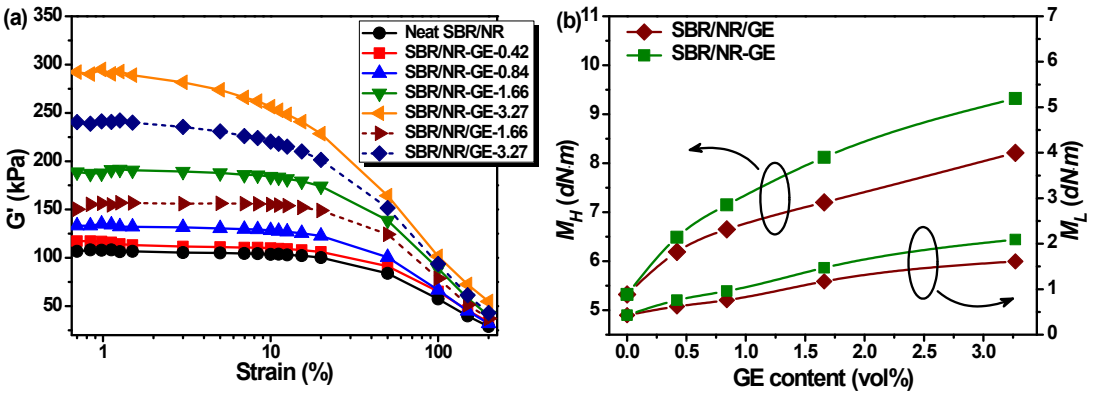

Fig. S6 (a) Dependence of the G′ of the uncured neat SBR/NR, SBR/NR-GE and SBR/NR/GE compounds on the strain, (b) M_L and M_H of the SBR composites.

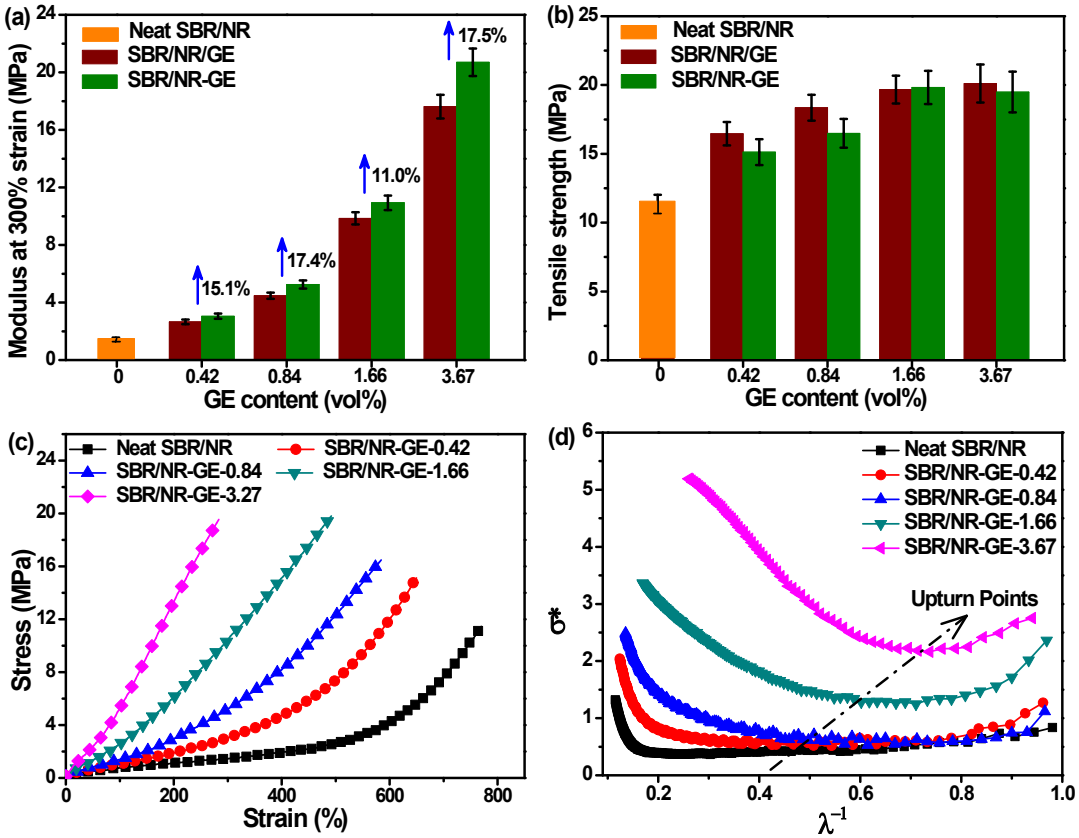

Fig. S7 (a) The modulus at 300% strain, (b) the tensile strength, and (c) the typical stress-strain curves of SBR/NR-GE. (d) σ^* as a function of λ^{-1} in the SBR/NR composites based on the Mooney-Rivlin equation.

The Mooney-Rivlin plots were performed to evaluate the elastomeric network by plotting the reduced stress (σ^*) against the reciprocal of the extension ratio (λ). The equation is listed as follow, $\sigma^* = \sigma/(\lambda - \lambda^{-2})$. As shown in Fig. S7(d), σ^* of composites presents a large and abrupt upturn at low λ^{-1}, which is attributable of the restriction of the mobility of the rubber chains. For all SBR/NR-GE samples, σ^* is dependent of λ upon deformation, which is because the strong interfacial adhesion between NR and *f*-GE can effectively constrain the mobility of the NR chains. It is clearly observed that the value of the λ^{-1} at which the upturn point shifts to lower extension ratios with increasing *f*-GE content. This is because that the increasing *f*-GE amount means a more developed interconnected network, leading to more restrictions on extensibility of the rubber chains. Such observations are consistent with the resulted analysis of the TEM observations.

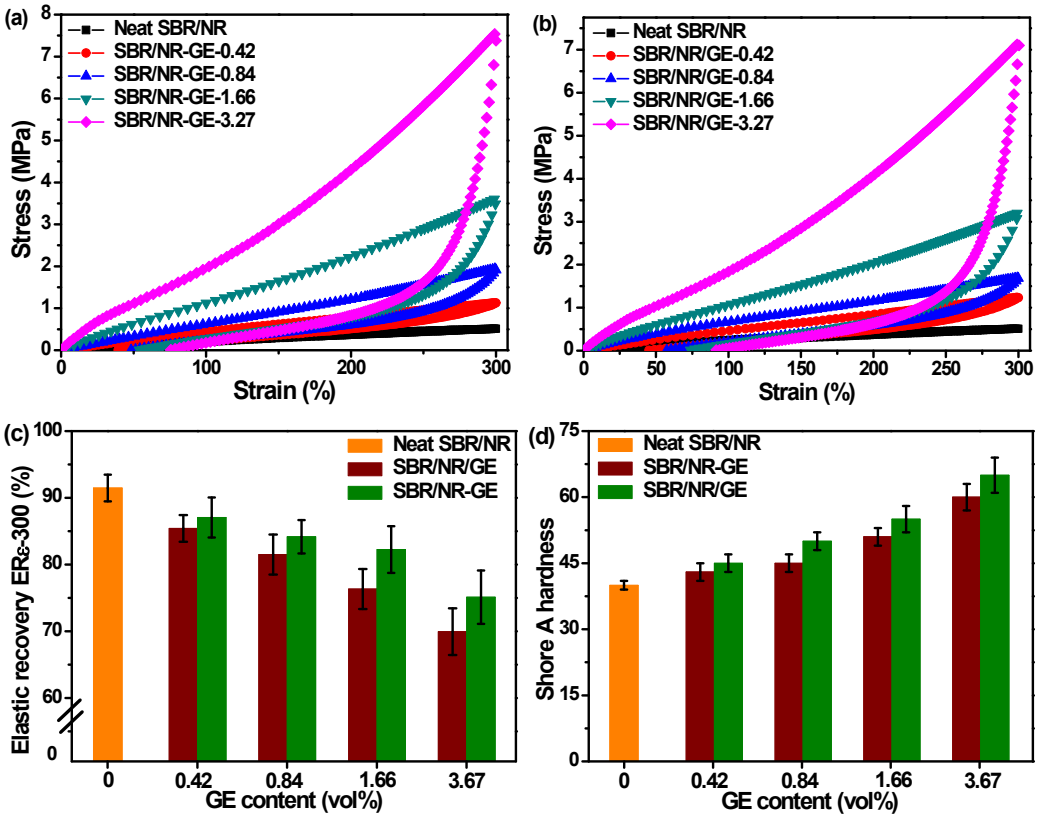

Fig. S8 (a and b) The representative extension-relaxation curves of SBR/NR-GE (a) and SBR/NR/GE (b) after 300% strain. (c and d) The elastic recovery after 300% strain (c) and Shore A hardness (d) of the double-interconnected SBR/NR-GE and non-interconnected SBR/NR/GE.

Table S1 The experimental formula for preparation of SBR/NR composites.

NO.	Neat	*f*-GE-0.25	*f*-GE-0.5	*f*-GE-0.75	*f*-GE-1.0	*f*-GE-2.0	*f*-GE-4.0
f-GE	0[α]	0.25	0.5	0.75	1.0	2.0	4.0
SBRL	83.4	83.4	83.4	83.4	83.4	83.4	83.4
NRL	83.4	83.4	83.4	83.4	83.4	83.4	83.4
ZnO	5	5	5	5	5	5	5
SA	2	2	2	2	2	2	2
MB	1	1	1	1	1	1	1
CZ	1.5	1.5	1.5	1.5	1.5	1.5	1.5
DM	0.5	0.5	0.5	0.5	0.5	0.5	0.5
S	1.5	1.5	1.5	1.5	1.5	1.5	1.5
OP-10	3	3	3	3	3	3	3

[α] parts per hundred parts of rubber

Table S2 The comparison of electrical behavior (*e.g.* percolation threshold, the corresponding conductivity) of GE/elastomer composites previously reported.

Rubber	Filler	Percolation threshold	Conductivity ($S \cdot m^{-1}$)	Ref.
NR	GE	0.62 vol%	$\sim 10^{-7}$	8
SBR	GE	~1.76 vol%	$\sim 10^{-7}$	9
NR	GE	0.21 vol%	$\sim 10^{-8}$	10
SBR	GE	0.55 vol%	$\sim 10^{-8}$	2
TPU[a]	GE	0.05 vol%	$\sim 10^{-11}$	11
ENR[b]	GE	0.23 vol%	$\sim 10^{-10}$	12
SBR/NR	GE	0.30 vol%	$\sim 10^{-7}$	This work

[a] Thermoplastic polyurethane;

[b] Epoxidized natural rubber.

Table S3 Strain sensors based on elastomer composites previously reported.

Matrix	Filler	Max strain (%)	Gauge factor	Ref.
PDMS[a]	SWCNT	280	0.82	13
PDMS	CNT	150	0.004	14
PU[b]	MWCNT	403	4	15
PDMS	CNT	300	1	16
PDMS	GE/Nanocellulose	100	7.1	17
PDMS	AgNWs	70	14	18
NR	GE	800	35	19
PDMS	GaInSn	60	2	20
NR	CNT	100	43.5	21
PDMS	GE	7.1	14	22
TPE[c]	CB	80	20	23
PU	CNT	400	69	24
PDMS	CB	150	29.1	25
SBR/NR	GE	120	82.5	This work

[a] Polydimethylsiloxane;

[b] Polyurethane;

[c] Thermoplastic elastomer;

Notes and references

1 Y. Lin, S. Q. Liu, J. Peng and L. Liu, *Compos. Part A*, 2016, **86**, 19.

2 Y. Lin, S. Q. Liu and L. Liu, *J. Mater. Chem. C*, 2016, **4**, 2353.

3 Y. Wei, S. Chen, Y. Lin, X. Yuan and L. Liu, *J. Mater. Chem. C*, 2016, **4**, 935.

4 Y. Wei, S. Chen, X. Yuan, P. P Wang and L. Liu, *Adv. Funct. Mater.,* 2016, DOI: 10.1002/adfm.201600580

5 J. Kim, L. J. Cote, F. Kim, W. Yuan, K. R. Shull and J. Huang, *J. Am. Chem. Soc.*, 2010, **132**, 8180.

6 Z. Peng, C. Feng, Y. Luo, Y. Li and L. X. Kong, *Carbon*, 2010, **48**, 4497.

7 Z. Peng, L. X. Kong, S. D. Li, Y. Chen and M. F. Huang, *Compos. Sci. Technol.*, 2007, **67**, 3130.

8 Y. H. Zhan, M. Lavorgna, G. Buonocore and H. S. Xia, *J. Mater. Chem.*, 2012, **22**, 10464.

9 W. Xing, M. Z. Tang, J. R. Wu, G. S. Huang, H. Li, Z. Y. Lei, X. Fu and H. Y. Li, *Compos. Sci. Technol.*, 2014, **99**, 67.

10 Y. Y. Luo, P. F. Zhao, Q. Yang, D. N. He, L. X. Kong and Z. Peng, *Compos. Sci. Technol.*, 2014, **100**, 143.

11 H. Liu, Y. L. Li, K. Dai, G. Q. Zheng, C. T. Liu, C. Y. Shen, X. R. Yan, J. Guo and Z. H. Guo, *J. Mater. Chem. C*, 2016, **4**, 157.

12 C. Z. He, X. D. She, Z. Peng, J. P. Zhong, S. Q. Liao, W. Gong, J. H. Liao and L. X. Kong, *Phys. Chem. Chem. Phys.*, 2015, **17**, 12175.

13 T. Yamada, Y. Hayamizu1, Y. Yamamoto, Y. Yomogida, A. Izadi-Najafabadi, D. N. Futaba and K. Hata, *Nat. Nanotechnol.*, 2011, **6**, 296.

14 D. J. Lipomi, M. Vosgueritchian, B. C-K. Tee, S. L. Hellstrom, J. A. Lee, C. H. Fox and Z. Bao, *Nat. Nanotechnol.*, 2011, **6**, 788.

15 P. Slobodian, P. Riha and P. Saha, *Carbon*, 2012, **50**, 3446.

16 L. Cai, L. Song, P. Luan, Q. Zhang, N. Zhang, Q. Gao, D. Zhao, X. Zhang, M. Tu, F. Yang, W. Zhou, Q. Fan, J. Luo, W. Zhou, P. M. Ajayan and S. Xie, *Sci. Rep.,* 2013, **3**, 3048.

17 Ch. Yan, J. Wang, W. Kang, M. Cui, X. Wang, C. Foo, K. J. Chee and P. Lee, *Adv. Mater.*, 2014, **26**, 2022.

18 M. Amjadi, A. Pichitpajongkit, S. Lee, S. Ryu, and I. Park, *ACS Nano*, 2014, **8**, 5154.

19 C. S. Boland, U. Khan, C. Backes, A. O'Neill, J. McCauley, S. Duane, R. Shanker, Y. Liu, I. Jurewicz, A. B. Dalton and J. N. Coleman, *ACS Nano*, 2014, **8**, 8819.

20 R. Matsuzaki and K. Tabayashi, *Adv. Funct. Mater.*, 2015, **25**, 3806.

21 S. Wang, X. Zhang, X. Wu and C. Lu, *Soft Matter*, 2016, **12**, 845.

22 S.-H. Bae, Y. Lee, B. K. Sharma, H.-J. Lee, J.-H. Kim and J.-H. Ahn, *Carbon*, 2013, **51**, 236.

23 C. Mattmann, F. Clemens, G. Trőster, *Sensors*, 2008, **8**, 3719.

24 P. Slobodian, P. Riha, R. Benlikaya, P. Svoboda and D. Petras, *IEEE Sens. J.*, 2013, **13**, 4045.

25 N. Lu, C. Lu, S. Yang and J. Rogers, *Adv. Funct. Mater.*, 2012, **22**, 4044.